Title

Capturing Solvation Effects at a Liquid/Nanoparticle Interface by Ab Initio Molecular Dynamics: Pt201 Immersed in Water

Journal

Small, 12(38)

ISSN

1613-6810

Authors

de Morais, Rodrigo Ferreira
Kerber, Torsten
Calle-Vallejo, Federico
et al.

Publication Date

2016-10-01

DOI

10.1002/smll.201601307

Peer reviewed

DOI: 10.1002/ ((please add manuscript number))
Article type: Full Paper

Capturing Solvation Effects at a Liquid/Nanoparticle Interface by Ab Initio Molecular Dynamics: Pt_{201} Immersed in Water

*Rodrigo Ferreira de Morais, Torsten Kerber, Federico Calle-Vallejo, Philippe Sautet, and David Loffreda**

Dr Rodrigo Ferreira de Morais, Dr Torsten Kerber, Dr Federico Calle-Vallejo, Dr Philippe Sautet, Dr David Loffreda
Univ Lyon, Ens de Lyon, CNRS, Université Lyon 1, Laboratoire de Chimie UMR 5182, F-69342, Lyon, France.
Fax: +33.4.72.72.88.60; Tel: +33.4.72.72.88.43.
E-mail: david.loffreda@ens-lyon.fr

Dr Federico Calle-Vallejo
Leiden Institute of Chemistry, Leiden University, PO Box 9502, 2300 RA Leiden, The Netherlands.

Keywords: heterogeneous catalysis, nanoparticles, platinum/water interface, density functional theory, solvation effects

Abstract. Solvation can substantially modify the adsorption properties of heterogeneous catalysts. Although essential for achieving realistic theoretical models, assessing such solvent effects over nanoparticles is challenging from a computational standpoint due to the complexity of those liquid/metal interfaces. We investigate this effect by ab initio molecular-dynamics simulations at 350 K of a large platinum nanoparticle immersed in liquid water. The first solvation layer contains twice as much physisorbed water molecules above the terraces, than chemisorbed ones located only at edges and corners. The solvent stabilizes the binding energy of chemisorbates: 66 % of the total gain comes from interactions with physisorbed molecules and 34 % from the influence of bulk liquid.

1. Introduction

Interfaces between liquid water and nanoparticles (NPs) play a key role in nanotechnology. A comprehensive understanding of these interfaces is still challenging, both from experimental and theoretical standpoints.[1–4] For instance, platinum NPs supported on carbon agglomerates are the most common catalyst for the oxygen reduction reaction (ORR) in polymer electrolyte

membrane fuel cells (PEMFCs).[5] Although the effect of the support on the activity of those NPs has been investigated in theory,[6–11] the role of the solvent is rarely examined.[12] In fact, the experimental detection of the small number of water molecules at liquid/particle interfaces is difficult,[13,14] which is why model interfaces at single-crystal metal surfaces are typically studied.[2,13–20]

Simulating liquid water is challenging due to the combination of various effects, such as large permanent dipoles, strong polarizability effects and cooperativity of hydrogen bond networks.[2,16,21] Liquid water/metal interfaces increase the level of complexity since the interfacial water molecules exhibit different structural organization and energetics compared to bulk liquid. A reasonable description of liquid water is provided by *ab initio* molecular dynamics (AIMD), including the coexistence of two states of the liquid (low density liquid LDL vs high density liquid HDL). Non-local correlation functionals able to describe van der Waals (vdW) forces in AIMD simulations of water allow for a balanced description of the LDL-like structure, better described by PBE-GGA functional (tetrahedral structure), and the HDL-like structure, obtained by vdW-DF2 functional (more compact and less tetrahedral).[18]

The interaction of multilayers of water in contact with a metallic surface (from single molecule adsorption to ice-monolayers, bilayers etc) has been studied several times during the last decades.[15,17,22–27] Multiple forms of adsorption have been examined (from monomers to heptamers and multiple bilayers) with density functional theory (DFT) calculations.[23] The influence of the metal[23–25,27] and the choice of the methodology[2,26,27] have also been investigated. On Pt(111), the variation of the adsorption energy from monomer (flat chemisorption through the oxygen atom on top sites) to multiple bilayers (including H-up and H-down adsorption configurations) is in the range 0.3-0.6 eV.[23,28–31] Crossing over different metallic surfaces, the adsorption strength of the monomer changes from 0.1 to 0.4 eV.[23–25,27] The adsorption strength of the monomer is also significantly modified when different exchange-correlation functionals are considered (from 0.01 to 0.47 eV).[26–29,32] A last point of

comparison is the influence of water coverage on the adsorption energy, which is rather limited: from 0.2 to 0.4 eV in a coverage between 1/3 and 1/27 ML on Pd(111) (ML = monolayer), using PBE-GGA functional.[26] Finally hydrogen bonds between adsorbed dimers have also been evaluated on Pt(111): the stabilization depends non-linearly on the number of water adsorbates (from 0.06 to 0.2 eV).[23,28]

Implicit continuum models,[33,34] bilayer-based static or dynamic explicit solvation models[35–41] and confined thin-liquid systems[42–44] have been proposed to evaluate the chemical properties of water/Pt(111) interfaces. All these interesting studies have not focused on the effects of liquid water on the adsorption strength at the interface. Moreover, they have not assessed the influence of the catalyst morphology on the organization of the liquid in the interface region. The few theoretical works devoted to water adsorption on NPs dealt with water monomers adsorption on Pt NPs of various sizes in vacuum.[45,46] The results showed that single water molecules prefer to adsorb on the corner of NPs with a moderate adsorption strength around 0.5 eV.

In view of the need for realistic liquid/nanoparticle interface models under temperature and chemical potential conditions, we investigate here the adsorption and solvation properties at NP surfaces immersed in liquid water. We address this subject by means of AIMD simulations of a Pt NP with a diameter of ~2 nm surrounded by ~700 water molecules at 350 K. The evolution of the surface coverage of chemisorbed water molecules at the interface is determined. Solvation effects on water chemisorption energies are evaluated by examining the variation of the average interaction energy between a single chemisorbed water molecule and the platinum NP. Finally, we present an energy decomposition model to capture the main features of this phenomenon.

2. Results and Discussion

2.1. Interface Model

The interface model (**Figure 1**) has been built up (complete system in Figure 1a) by using the optimized geometry of a Pt_{201} nanoparticle (Figure 1d) and the resulting structure of liquid water equilibrated at 350 K after 100 picoseconds (ps) with AIMD and PBE functional (3D box with 50 molecules). For pure water, the size of the 3D box and the number of molecules in it have been chosen to reproduce the experimental density of water at 350 K, namely 0.98 g cm^{-3}.[58] The truncated octahedron shape of Pt_{201} has already been reported by experimental and theoretical works.[59] The initial configuration of the interface between the nanoparticle and the liquid has been built by duplicating the 3D box of equilibrated pure water and by extracting the water molecules included within the volume of a sphere corresponding to the diameter of Pt_{201}. The volume of the 3D box of the complete system (28×26×27 $Å^3$) has been calculated to obtain an equivalent density of water (0.98 g cm^{-3}) in the excluded volume at the interface with the nanoparticle, which is achieved when 698 explicit water molecules are in the box.

Before the MD simulation, the complete interface has been optimized at 0 K accurately by relaxing all the degrees of freedom of water and platinum with PBE. Tests with non-local dispersion corrected functionals (namely vdW-DF2 and BEEF-vdW) have been performed to evaluate the influence on the interaction energy of chemisorbed water at the liquid/nanoparticle interface. According to our tests, the non-local dispersion-corrected functionals increase the optimal volume of the nanoparticle (12 % for vdW-DF2 and 2 % for BEEF-vdW) (see section S2 in the Supporting Information (SI)). Hence the PBE offers the best compromise for describing at the same time the tetrahedral model for the liquid state of water (LDL) and reasonable Pt nanoparticle volume, with respect to bulk references.

2.2. Molecular Dynamics Simulations

The total potential energy and the moving average (considering time windows of 50 femtoseconds) for the surface coverage of chemisorbed water (θ_{H2O}) (**Figure 2**) are plotted along the 4 ps trajectory of the AIMD simulation. After the first picosecond (thermalization), statistics can be registered along the remaining 3 ps. During that interval of time, the variations of the potential energy (~13 meV per water molecule) and of the moving average of the surface coverage (~0.0075 ML corresponding to a global increase of 6 chemisorbed water molecules between 0 and 4 ps) are small, hence justifying the relevance of registering statistics. During the total simulation time, more than 100 events took place on the nanoparticle surface: 54 water adsorption and 48 desorption events. Between 1 and 2 ps, a first plateau is reached in coverage, which subsequently increases slightly between 2 and 3 ps to reach a second plateau after 3 ps. Hence, meaningful statistics can be extracted from the those two plateaus, where constant coverage is found (equilibrated configurations). Note in passing that the observed surface coverage (0.286 and 0.292 ML for the two plateaus, corresponding to 35 and 36 water molecules adsorbed on 122 surface platinum atoms) are close to experimental estimations of surface coverage of oxygenated species at relevant PEMFC potentials on Pt(111), and Monte-Carlo simulations based on DFT parameters.[60,61]

During the MD simulation, a strong reorganization of the chemisorbed layer has been observed, with several adsorption desorption processes. Figure 2 shows a progressive desorption of the water molecules initially located at the center of the terraces in favor of exclusive chemisorption on the NP corners and edges. During the last picosecond, the first solvation layer is composed of almost twice as much physisorbed water molecules than chemisorbed ones. At 0 K, the Pt-O optimal distance for chemisorbed water at the corner of Pt_{201} in vacuum is 2.2 Å, whereas in liquid conditions at 350 K, the corresponding bond length is in the range 2.2-2.6 Å.

2.3. Averaged Electrostatic Potential

From the standpoint of classical physics, the energetics of interface water molecules can essentially result from electrostatic and covalent interactions or from van der Waals forces. The electrostatic component is provided (**Figure 3**). The spherically averaged electrostatic potential ξ is plotted along the radius of the NP, starting from its center of mass up to the external border of the liquid box (Figure 3b), together with the radial distribution of water molecules within the 3D box (Figure 3a). Note that this particular choice of representation enables a straightforward decoupling of the contributions to the average potential coming from the NP, the chemisorbed and physisorbed water molecules, and the bulk water. The average electrostatic potential in the region of the metal shows 4 minima (at 0, 2.5, 5.8 and 7.7 Å) corresponding to the various NP shells. Furthermore, in the interface region, there is a first local minimum at 10.7 Å due to the first solvation layer. In the radial distribution, the first two peaks at 10.3 and 10.7 Å correspond to the chemisorbed and physisorbed water molecules, respectively. In the chemisorbed layer containing 37 molecules, the water is bound to the NP surface through the oxygen lone pairs with the plane formed by the hydrogen and oxygen atoms almost parallel to the NP surface (flat configuration). Chemisorption happens exclusively at corner and edge sites, which can be understood in terms of the lower coordination number of these sites in comparison to the low-index terraces.[46] The physisorbed layer (79 molecules) is a mixture of H-up and H-down oriented water molecules: the former exhibit one O-H bond toward the NP surface, whereas the latter form a network of hydrogen bonds with no preferential orientation, in opposition to the well-known structure of ice-like bilayers (hexagonal (Ih) or cubic (Ic) conformations, as reported from LEED and low temperature STM studies[2,15,17,22]). Similar characteristics of the first contact layer have been reported recently for water/Pt(111) with classical MD simulations.[62] Above 12 Å, the weak oscillations of the average electrostatic potential are attributed to the bulk water shells, the expected long-range density oscillations of which cannot be captured in this first modeling.

2.4. Energy Decomposition Analysis and Interaction Energy

Energy decomposition analyses (EDAs) are an interesting approach to understand the impact of solvation on adsorption energetics and average electrostatic potential (**Figure 4**). Usually EDAs split the adsorption energy in two different contributions: interaction and deformation terms.[63–65] The interaction term represents the energy associated with the formation of a chemical bond, at constant final geometry for both interacting species, while the deformation energy is the cost to adapt the optimal geometry of the isolated species to the situation in which the bond is formed (see section S1 in the SI). In vacuum, the latter contribution (water and NP deformations) is negligible for water monomer adsorption on the platinum NPs of various sizes and extended surfaces, due to the small geometry distortions associated with chemisorption. Although in liquid conditions those contributions are substantial, their evaluation is hardly accessible due to the large number of subsystems to consider and to the required simulation time. Thus, in the following, we focus exclusively our analysis on the interaction energy contributions, namely those related to the effective chemical bonding. For water monomer chemisorption at a corner (which is the most stable binding site on Pt_{201}), the interaction energy is -0.54 eV, in the range 0-350 K. This value is similar to the adsorption energy on Pt_{201} in vacuum (-0.49 eV).[46,65] The effect of the complete co-chemisorbed layer of water molecules (36 molecules in average) destabilizes the interaction energy to -0.13 eV at 350 K. This is expected as the coverage increases (lateral destabilizing interactions between water chemisorbates without hydrogen bonds). The effect of the physisorbed molecules belonging to the first solvation layer is strongly stabilizing, with a gain of -0.92 eV leading to an interaction energy of -1.05 eV at 350 K. The full system is completed by the bulk water molecules, which increases the interaction energy of a single chemisorbed water molecule at the corner to -1.52 eV (hence corresponding to a gain of -0.47 eV). In summary, the complete gain of interaction energy combining both the first solvation layer (physisorbed molecules)

and the rest of the liquid (bulk molecules) is -1.39 eV per water molecule. This significant gain due to solvation comes from the first solvation layer (contribution of 66%) and the other liquid layers (contribution of 34 %). The formation of hydrogen bonds between the chemisorbed water and some of the physisorbed water molecules is largely responsible for the major gain in interaction energy.

In order to validate this model, we have examined other liquid water/platinum nanoparticle interfaces (with Pt_{38}, Pt_{55}, Pt_{68}, Pt_{79}) through AIMD simulations. Those NPs present different morphology or size than Pt_{201}. Among those cases, $Pt_{68}/(H_2O)_{302}$ keeps sufficiently intact its geometry at 350 K during the 4 ps, similar to $Pt_{201}/(H_2O)_{698}$. Pt_{68} is a regular truncated tetrahedron exhibiting large hexagonal and small triangular (111) facets, the structures of which are only weakly modified during the AIMD simulations at 350 K. The other NPs (Pt_{38}, regular truncated octahedron and Pt_{79}, irregular truncated octahedron) possess square (100) facets, the structures of which are significantly modified along the trajectory at 350 K. In these cases, the small square facets composed of 4 atoms undergo deformations from square to rhombic symmetries. Therefore adsorption-desorption statistics at 350 K may be biased by such distortions, hence making difficult the comparison with the $Pt_{201}/(H_2O)_{698}$ interface. Pt_{55} (regular cuboctahedron) has larger square (100) facets (composed of 9 atoms) than Pt_{38} and Pt_{79}, but small triangular (111) facets (composed of 6 atoms). Immersed Pt_{55} square facets undergo also significant deformations at 350 K, unlike Pt_{201}. Consequently, its corresponding adsorption-desorption statistics have not been considered either. For immersed Pt_{68} NP, the average coverage during the last picosecond is 0.345 ML, slightly larger than the one found for Pt_{201} (0.292 ML). The number of co-chemisorbed water molecules (20) has increased with respect to the total number of molecules in the 3D box (302), hence leading to a slightly larger fraction of 7% (5% for the interface with Pt_{201}). In contrast, the number of co-physisorbed molecules (54) has significantly increased referred to the total number of water molecules (a fraction of 18% for Pt_{68} vs 11% for Pt_{201}). This modification of the first solvation

layer is essentially due to the change of the NP morphology. The interface with the truncated tetrahedron nanoparticle (Pt_{68}) presents a curvature with a smaller diameter than the one with the truncated octahedron (Pt_{201}). The same EDA approach has been applied to the $Pt_{68}/(H_2O)_{302}$ system (Figure 4) and has shown an interaction energy of -0.61 eV for the water monomer at a corner of Pt_{68} (similar value to Pt_{201}). The effect of coverage (co-chemisorbed water) destabilizes the interaction energy of that water monomer in the same extent as Pt_{201} (-0.14 eV vs -0.13 eV, for Pt_{68} and Pt_{201}, respectively). This corresponds to a loss of stability of +0.47 eV for Pt_{68}, with respect to water monomer (+0.41 eV for Pt_{201}). The difference of loss from Pt_{68} to Pt_{201} is consistent with the increase of coverage. The influence of co-physisorbed water molecules belonging to the first solvation layer stabilizes the interaction energy of the chemisorbed water (-0.64 eV) likewise the interface with Pt_{201} (-1.05 eV), but to a lesser extent. This smaller energetic gain is justified by the change of morphology (truncated tetrahedron) which is less favorable for developing a network of hydrogen bonds. The rest of the bulk liquid stabilizes further the interaction energy to -1.04 eV, likewise Pt_{201}. As a summary, the whole energetic gain due to the first solvation layer (physisorbed and bulk water) is moderately smaller for Pt_{68} (-0.90 eV) than the one for Pt_{201} (-1.39 eV). The interesting result is the similar trend and ordering found for both interfaces, although the size and morphology of the NP have changed concomitantly. In fact, 56% of the gain is due to physisorbed water of the first solvation layer (66% for Pt_{201}), while 44% comes from the rest of the bulk liquid (34% for Pt_{201}).

Another important validation is the choice of the computational method. For $Pt_{201}/(H_2O)_{698}$, Figure 4 shows that all the interaction energies calculated with non-local or semi-empirical dispersion-corrected functionals at constant geometry are systematically stabilized by an equivalent amount from one subsystem to another (the stabilizing effect due to vdW interactions is in the range 0.21-0.44 eV). As those deviations are weaker than the variations of the interaction energy between one subsystem to the next, our global conclusions

are still valid regardless of the choice of exchange-correlation (XC) functionals (see Table S2 in the SI). Our trends in interaction energy support previous studies of ORR adsorption properties using implicit solvation models.[33] Alternatively, one can evaluate the interaction energy with a frozen liquid/nanoparticle interface completely relaxed at 0 K (Figure 4e). In this case, the interaction energy (-1.09 eV) is not as large as the one calculated at 350 K (-1.52 eV). Hence, neglecting temperature effects causes an error of 0.43 eV with respect to the complete system at 350 K.

3. Conclusion

Summarizing, in this work, we analyze solvation effects at a liquid water/platinum nanoparticle interface at 350 K using AIMD simulations and an energy decomposition model. During the MD, a progressive reorganization of the solvation layer at the interface is observed with an exclusive chemisorption of water at undercoordinated sites of the nanoparticle, such as corners and edges. This occurs through a series of simultaneous adsorption and desorption processes at different locations of the nanoparticle. The solvation layer exhibits a complex mixture of H-up and H-down physisorbed water molecules with no specific intermolecular orientation, in contrast with ice-like bilayers, typically used in the literature to model water networks on extended platinum surfaces. We have rationalized these solvation effects from a classical standpoint, using the average electrostatic potential along the nanoparticle radius up to the liquid bulk. A remarkable stabilization of the electrostatic potential has been found in the region of the solvation layer. The EDA model suggests that the interaction energy between a reference water monomer at a nanoparticle corner and Pt_{201} is significantly increased because of physisorbed and liquid bulk molecules. Thus, solvation tends to strengthen the chemical bonding of chemisorbed water with the nanoparticle surface. In contrast, co-chemisorbed molecules tend to destabilize the interaction energy of reference water monomer. Notably, we show that these conclusions do not depend on the choice of XC functionals. This

work shows the relative importance of various solvation layers on adsorption energetics at liquid/nanoparticle interfaces. Based on this insight, new coupled methods with restricted quantum descriptions of the liquid could be developed. Longer MD simulations could then be explored to determine solvent/adsorbate effects at realistic liquid/nanoparticle interfaces.

4. Experimental Section

Density functional theory calculations have been performed with the Vienna Ab initio Simulation Package (VASP)[47,48] using periodic boundary conditions. The generalized gradient approximation (GGA) has been used with the Perdew-Burke-Ernzerhof (PBE) exchange-correlation functional[49] and the projector augmented-wave method (PAW).[50] Interaction energies have also been calculated with various other functionals including van der Waals forces: Bayesian Error Estimation Functional (BEEF-vdW),[51] van der Waals density functional (vdW-DF2),[52] semi-empirical Grimme's DFT-D2 (D2(0))[53] and zero damping DFT-D3 (D3(0)),[54] Becke-Jonson damping DFT-D3 (D3(BJ))[55] and Tkatchenko-Scheffler (TS)[56] methods. The energy cut-off has been set to 400 eV throughout the study. The criterion related to total electronic energy convergence was set to $\pm 10^{-6}$ eV. A tight convergence for the geometry optimizations has been ensured by a threshold of $\pm 10^{-2}$ eV Å^{-1} for the residual forces acting on the nuclei. The gamma point only approach has been used to describe the Brillouin zone. Ab initio molecular dynamics (AIMD) within the Born-Oppenheimer (BO) approximation has been also performed using VASP code in the canonical ensemble (NVT) to simulate the equilibration of the liquid/nanoparticle interface. The Nosé-Hoover thermostat has been used to maintain the temperature constant at 350 K.[57] The time step for the integration of classical equations of motion of the nuclei has been set to 1 fs (femtosecond) with a complete trajectory integrated up to 4 picoseconds (ps) (corresponding to 4000 different structures of the interface). The interaction energy between one water molecule and the platinum nanoparticle is presented in section S1 of SI. The chemisorption of

water is defined by the interaction of one molecule with surface platinum atoms through oxygen (Pt-O distances shorter than 2.6 Å), whereas the physisorption by the interaction through hydrogen atoms (Pt-O distances in the range 2.6-3.6 Å). The water coverage θ is defined as the ratio between the total numbers of chemisorbed water molecules and nanoparticle surface atoms and is expressed in monolayer (ML).

Supporting Information

Details about the energy decomposition analysis, effect of dispersion forces and Bader analysis are addressed in the Supporting Information.

Acknowledgements

The authors acknowledge the funding from the European Union FP7/2007-2013 program (PUMA MIND contract, Call FCH-JU-2011-1, Code SP1-JTI-FCH-2011.1.3, grant agreement number 303419). They thank IDRIS, CINES (project 609, GENCI/CT8) and PSMN for CPU time and assistance. FCV acknowledges funding from Netherlands Organization for Scientific Research (NWO), Veni project number 722.014.009.

Received: ((will be filled in by the editorial staff))
Revised: ((will be filled in by the editorial staff))
Published online: ((will be filled in by the editorial staff))

[1] F. Zaera, *Chem. Rev.* **2012**, *112*, 2920–2986.

[2] J. Carrasco, A. Hodgson, A. Michaelides, *Nat. Mater.* **2012**, *11*, 667-674.

[3] Z.-C. Zhang, B. Xu, X. Wang, *Chem. Rev.* **2014**, *43*, 7870-78886.

[4] F. Viñes, J. R. B. Gomes, F. Illas, *Chem. Soc. Rev.* **2014**, *43*, 4922-4939.

[5] L. Carrette, K. A. Friedrich, U. Stimming, *ChemPhysChem* **2000**, *1*, 162-193.

[6] Y. Okamoto, *Chem. Phys. Lett.* **2006**, *420*, 382-386.

[7] N. T. Cuong, A. Fujiwara, T. Mitani, D. H. Chi, *Comp. Mat. Sci.* **2008**, *44*, 163-166.

[8] T. Home, Y. Zhou, R. Pasquarelli, R. O'Hayre, *Phys. Chem. Chem. Phys.* **2010**, *12*, 9461-9468.

[9] D.-H. Lim, J. Wilcox, *J. Phys. Chem. C* **2012**, *116*, 3653-3660.

[10] Z. Zhao, L. Dubau, F. Maillard, *J. Power Sources* **2012**, *217*, 449-458.

[11] Z. Cheng, C. S. Lo, *Ind. Eng. Chem. Res.* **2013**, *52*, 15447-15454.

[12] U. Benedikt, W. B. Schneider, A. A. Auer, *Phys. Chem. Chem. Phys.* **2013**, *15*, 2712-2724.

[13] E. Johnson, *Science* **2002**, *296*, 477-478.

[14] J. T. J. Yates, C. T. Campbell, *Proc. Natl. Acad. Sci. USA* **2011**, *108*, 911-916.

[15] M. A. Henderson, *Surf. Sci. Rep.* **2002**, *46*, 1-308.

[16] C. Huang, K. T. Wikfeldt, T. Tokushima, D. Nordlund, Y. Harada, U. Bergmann, M. Niebuhr, T. M. Weiss, Y. Horikawa, M. Leetmaa, M. P. Ljungberg, O. Takahashi, A. Lenz, L. Ojamäe, A. P. Lyubartsev, S. Shin, L. G. M. Pettersson, A. Nilsson, *Proc. Natl. Acad. Sci. USA* **2009**, *106*, 15214-15218.

[17] A. Hodgson, S. Haq, *Surf. Sci. Rep.* **2009**, *64*, 381-451.

[18] A. Nilsson, L. Pettersson, *Chem. Phys.* **2011**, *389*, 1-34.

[19] T. Schiros, K. J. Andersson, J. MacNaughton, J. Gladh, A. Matsuda, H. Öström, O. Takahashi, L. G. M. Pettersson, A. Nilsson and H. Ogasawara, *J. Chem. Phys.* **2013**, *138*, 234708.

[20] K. Motobayashi, L. Arnadóttir, C. Matsumoto, H. J. E. M. Stuve, Y. Kim and M. Kawai, *ACS Nano* **2014**, *8*, 11583-11590.

[21] T. D. Kühne, M. Krack, M. Parrinello, *J. Chem. Theory Comput.* **2009**, *5*, 235-241.

[22] P. A. Thiel, T. E. Madey, *Surf. Sci. Rep.* **1987**, *7*, 211-385.

[23] S. Meng, E. G. Wang, S. Gao, *Phys. Rev. B* **2004**, *69*, 195404.

[24] P. Vassilev, R. A. van Santen, M. T. M. Koper, *J. Chem. Phys.* **2005**, *122*, 054701.

[25] A. Michaelides, *Appl. Phys. A* **2006**, *85*, 415-425.

[26] A. Poissier, S. Ganeshan, M. V. Fernández-Serra, *Phys. Chem. Chem. Phys.* **2011**, *13*, 3375-3384.

[27] R. Nadler, J. F. Sanz, *J. Mol. Model* **2012**, *18*, 2433-2442.

[28] P. Tereshchuk, J. L. F. D. Silva, *J. Phys. Chem.* **2013**, *117*, 16942-16952.

[29] J. Carrasco, J. Klimeš**,** A. Michaelides, *J. Chem. Phys.* **2013**, *138*, 024708.

[30] D. Loffreda, M. Michel, F. Delbecq, P. Sautet, *J. Catal.* **2013**, *308*, 374-385.

[31] M. J. Kolb, F. Calle-Vallejo, L. B. F. Juurlink, M. T. M. Koper, *J. Phys. Chem.* **2014**, *140*, 134708.

[32] I. Hamada, S. Meng, *Chem. Phys. Lett.* **2012**, *521*, 161-166.

[33] Y. Sha, T. H. Yu, Y. Liu, B. V. Merinov, W. A. Goddard, J. *Phys. Chem. Lett.* **2010**, *1*, 856-861.

[34] S. Sakong, M. Naderian, K. Mathew, R. G. Hennig, A. Groß, *J. Chem. Phys.* **2015**, *142*, 234107.

[35] T. Jacob, W. A. Goddard, *J. Am. Chem. Soc.* **2004**, *126*, 9360-9368.

[36] Y. Wang, P. B. Balbuena, *J. Phys. Chem. B* **2004**, *108*, 4376-4384.

[37] Y. Wang, P. B. Balbuena, *J. Phys. Chem. B* **2005**, *109*, 14896-14907.

[38] J. G. Wang, B. Hammer, *J. Chem. Phys.* **2006**, *124*, 184704.

[39] L. Ou, F. Yang, Y. Liu, S. Chen, *J. Phys. Chem. C* **2009**, *113*, 20657-20665.

[40] V. Tripkovic, E. Skúlasona, S. Siahrostamia, J. K. Nørskov, J. Rossmeisl, *Electrochim. Acta* **2010**, *55*, 7975-7981.

[41] T. Roman, A. Groß, *Catal. Today* **2013**, *202*, 183-190.

[42] T. R. Mattsson, S. J. Paddison, *Surf. Sci.* **2003**, *544*, L697-L702.

[43] M. Otani, I. Hamada, O. Sugino, Y. Morikawa, Y. Okamoto, T. Ikeshoji, *Phys. Chem. Chem. Phys.* **2008**, *10*, 3609-3612.

[44] K.-Y. Yeh, M. J. Janik, *J. Comp. Chem.* **2011**, *32*, 3399-3408.

[45] J. L. C. Fajín, A. Bruix, M. N. D. S. Cordeiro, J. R. B. Gomes, F. Illas, *J. Chem. Phys.* **2012**, *137*, 034701.

[46] F. Calle-Vallejo, J. I. Martinez, J. M. Garcia-Lastra, P. Sautet, D. Loffreda, *Angew. Chem. Int. Ed.* **2014**, *53*, 1-5.

[47] G. Kresse, J. Furthmüller, *Comp. Mat. Sci.* **1996**, *6*, 15-50.

[48] G. Kresse, J. Furthmüller, *Phys. Rev. B* **1996**, *54*, 11169-11186.

[49] J. P. Perdew, K. Burke, M. Ernzerhof, *Phys. Rev. Lett.* **1996**, *77*, 3865-3868.

[50] G. Kresse, D. Joubert, *Phys. Rev. B* **1999**, *59*, 1758-1775.

[51] J. Wellendorff, K. T. Lundgaard, A. Møgelhoj, V. Petzold, D. D. Landis, J. K. Nørskov, T. Bligaard, K. W. Jacobsen, *Phys. Rev. B* **2012**, *85*, 235149.

[52] K. Lee, E. D. Murray, L. Kong, B. I. Lundqvist, D. C. Langreth, *Phys. Rev. B* **2010**, *82*, 081101.

[53] S. Grimme, *J. Comp. Chem.* **2006**, *27*, 1787-1799.

[54] S. Grimme, J. Antony, S. Ehrlich and H. Krieg, *J. Chem. Phys.* **2010**, *132*, 154104.

[55] S. Grimme, S. Ehrlich, L. Goerigk, *J. Comp. Chem.* **2011**, *32*, 1456-1465.

[56] A. Tkatchenko, M. Scheffler, *Phys. Rev. Lett.* **2009**, *102*, 073005.

[57] D. Frenkel, B. Smit, Understanding Molecular Simulation, Second Edition: From Algorithms to Applications, Academic Press, **2001**.

[58] D. R. Lide, CRC Handbook of Chemistry and Physics, Vol. 90, CRC Press, Boca Raton, FL, **2009-2010**.

[59] L. Y. Chang, A. S. Barnard, L. C. Gontard, R. E. Dunin-Borkowski, *Nano Lett.* **2010**, *10*, 3073-3076.

[60] V. R. Stamenkovic, B. Fowler, B. S. Mun, G. Wang, P. N. Ross, C. A. Lucas, N. M. Markovic, *Science* **2007**, *315*, 493-497.

[61] H. S. Casalongue, S. Kaya, V. Viswanathan, D. J. Miller, D. Friebel, H. A. Hansen, J. K. Nørskov, A. Nilsson, H. Ogasawara, *Nat. Commun.* **2013**, *4*, 1-6.

[62] S. Duan, X. Xu, Z.-Q. Tian, Y. Luo, *Phys. Rev. B* **2012**, *86*, 045450.

[63] C. Morin, D. Simon, P. Sautet, *J. Phys. Chem. B* **2004**, *108*, 5653-5665.

[64] S. Laref, Y. Li, M.-L. Bocquet, F. Delbecq, P. Sautet, D. Loffreda, *Phys. Chem. Chem. Phys.* **2011**, *13*, 11827-11837.

[65] F. Calle-Vallejo, P. Sautet, D. Loffreda, *J. Phys. Chem. Lett.* **2014**, *5*, 3120-3124.

Figure 1. Interface between liquid water and a platinum nanoparticle extracted from the AIMD trajectory at 350 K after 4 ps. a) Complete system composed of a Pt_{201} nanoparticle (truncated octahedron shape) immersed in a 3D box containing 698 explicit water molecules. b) Water physisorbed layer composed of 72 molecules in contact with the NP (Pt-O bonds in the range 2.6-3.6 Å). c) Water chemisorbed layer composed of 38 molecules at the nanoparticle surface (Pt-O bonds shorter than 2.6 Å). d) NP in vacuum, composed of 14 facets (8 hexagonal (111)-type and 6 square (100)-type) with a diameter of 1.7 nm, and the thickness of the liquid being considered in two directions. Platinum atoms are represented in dark (terraces) and light (edges and corners) blue, while oxygen appears in red and hydrogen in white.

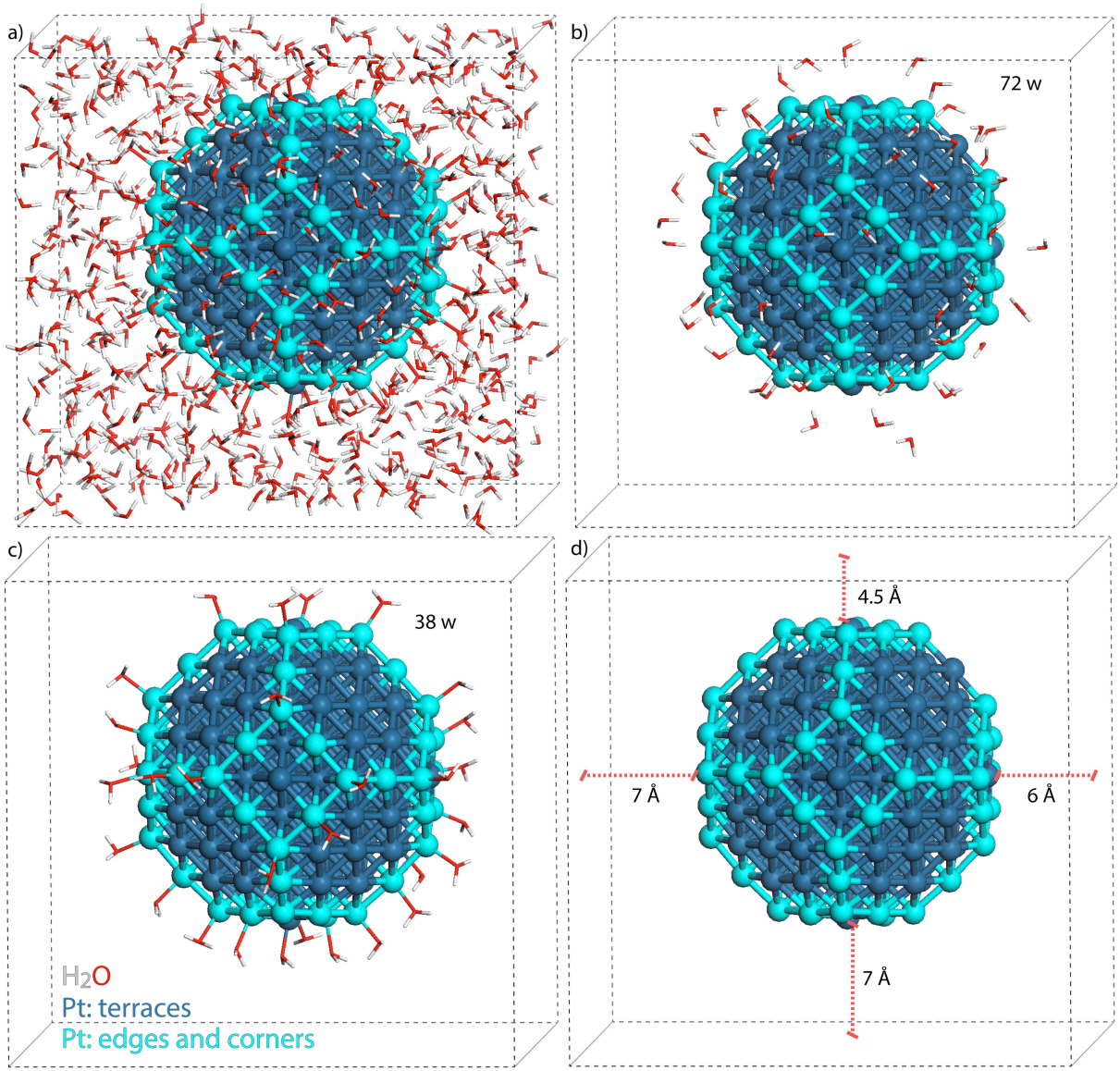

Figure 2. Total potential energy V (eV, blue curve) and surface coverage θ (ML = monolayer, red curve) plotted along the AIMD trajectory of 4 ps at 350 K. V is normalized per water molecule and referenced to the energy of the initial 0 K relaxed interface. θ is an incremental moving average defined as the ratio between the total numbers of chemisorbates and nanoparticle surface atoms. During the MD, an increase of chemisorbed water from 31 to 37 molecules is observed mainly on undercoordinated NP sites (corners and edges). The atom labels are those of Figure 1.

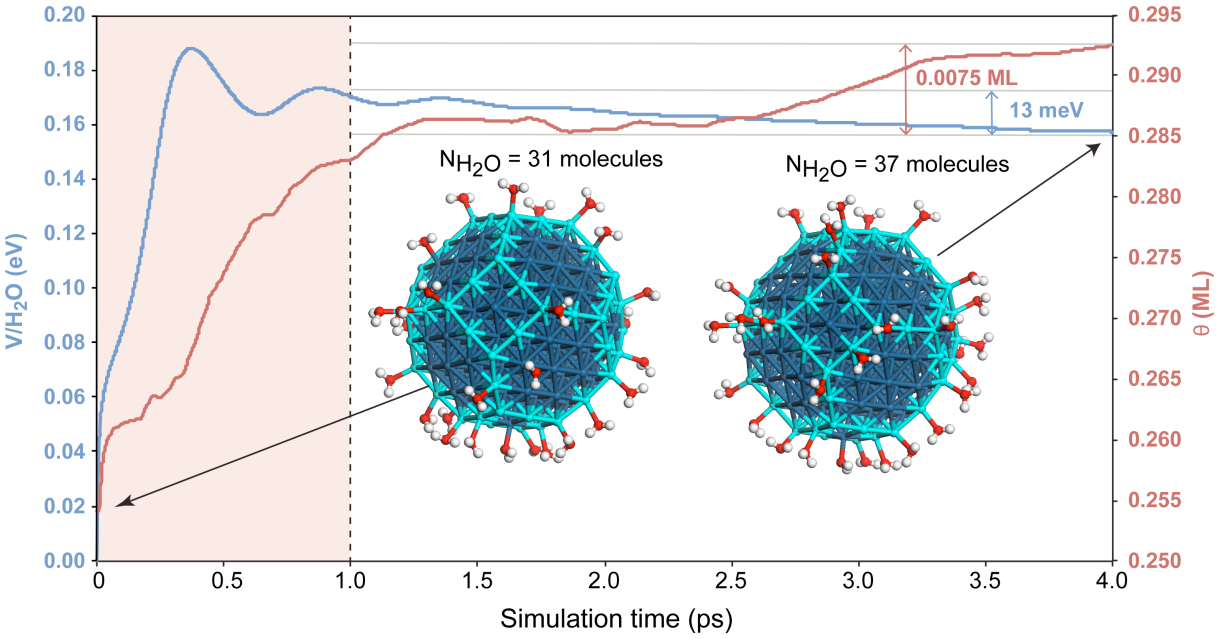

Figure 3. a) Radial distribution of water molecules N_{H2O} defined from the center of mass of the nanoparticle. b) Spherically averaged electrostatic potential ξ (eV) defined from the center of mass of the nanoparticle. The two properties have been averaged over the last picosecond of the MD trajectory at 350 K. Platinum atoms of the nanoparticle (N.P.) are represented in blue, oxygen and hydrogen of water molecules (chemisorbed χ and physisorbed φ) in red and white, respectively.

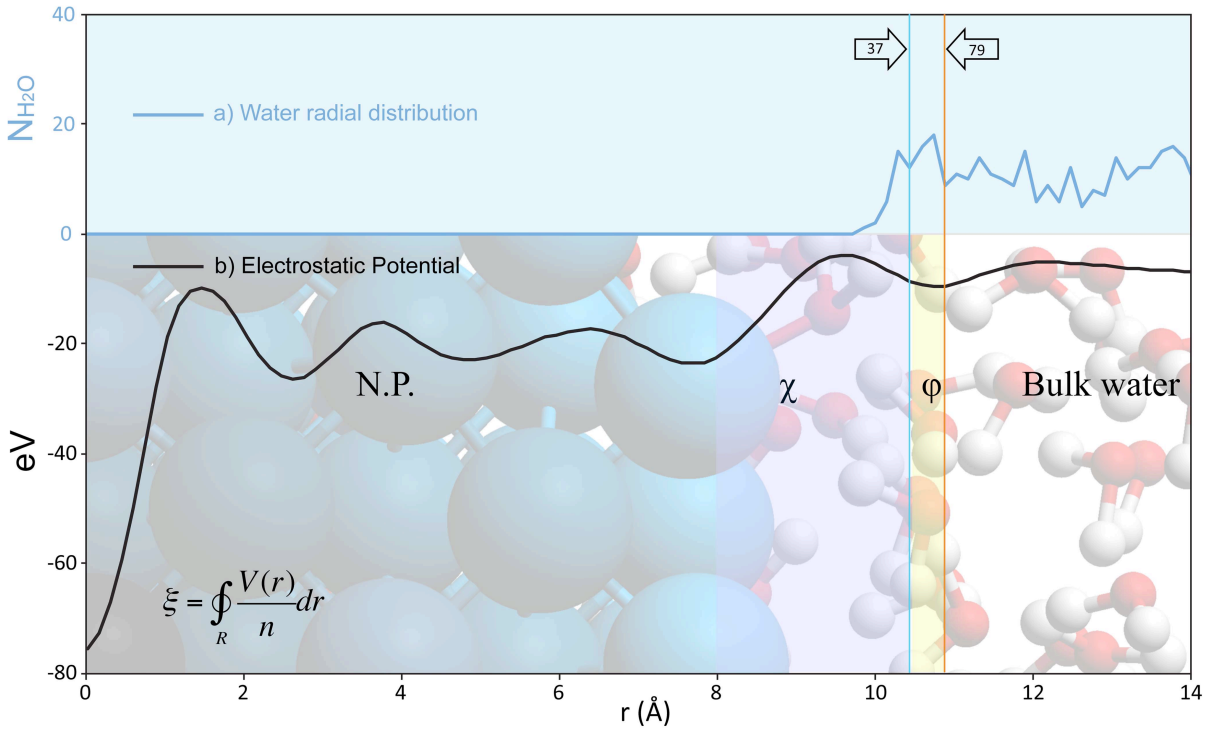

Figure 4. Energy decomposition model for the interaction energy E_{INT} (eV) between the platinum nanoparticle and one water molecule (indicated by a red circle) chemisorbed on a NP corner (GGA-PBE). This molecule is chemisorbed: a) in vacuum on the bare NP at 0 or 350 K; d) in liquid condition at 350 K; e) in "frozen" condition at 0 K (completely relaxed interface). The solvation effect is decomposed by considering several subsystems of the complete interface: b) complete co-chemisorbed layer in vacuum at 350 K; c) complete co-physisorbed layer belonging to the first solvation layer, in vacuum at 350 K. All interaction energies have been averaged over the last picosecond of the MD trajectory, except a) and e) at 0 K. The atom labels are those defined in Figure 1. The colored areas define the stabilizations $\boldsymbol{\delta}_{vdW}$ (eV) of those energies when considering dispersion-corrected functionals (either non-local or semi-empirical).

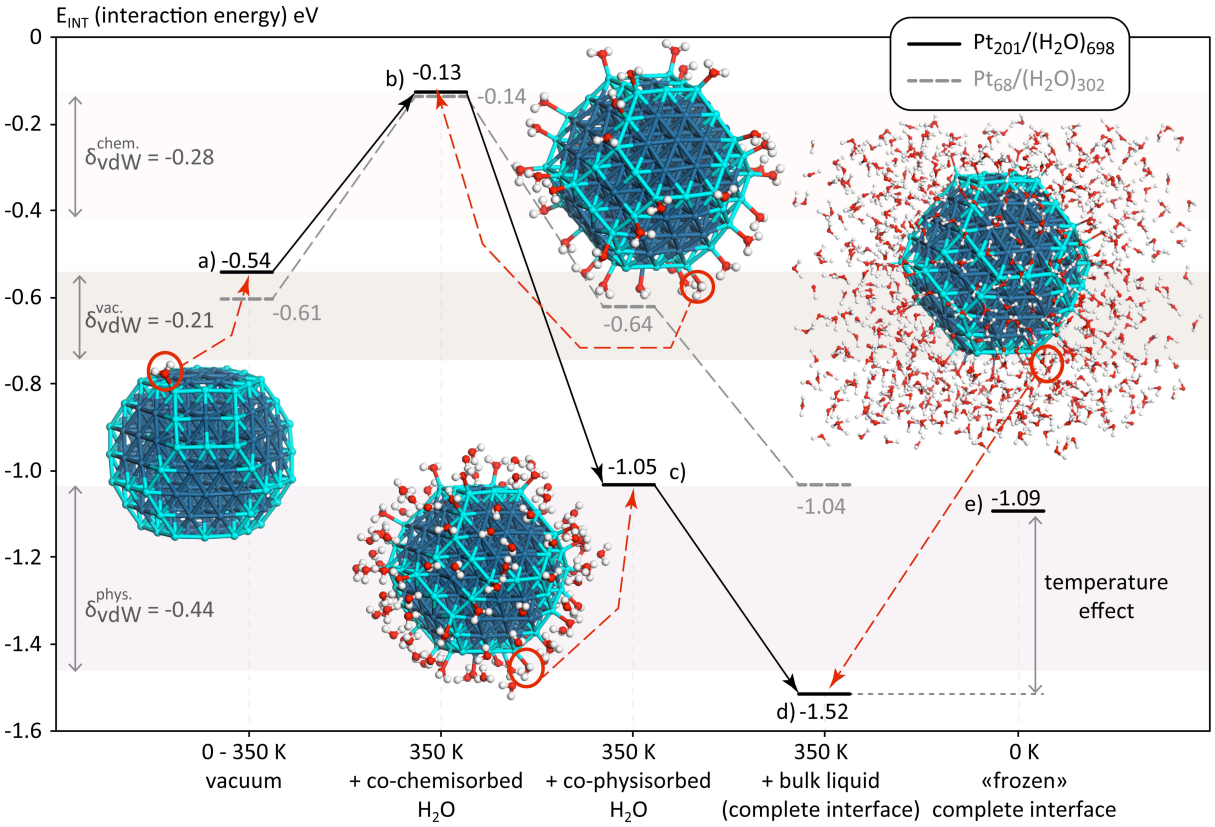

Ab initio molecular dynamics simulations are proposed to investigate the solvation effects at the interface between a platinum nanoparticle (Pt_{201}) and liquid water at 350 K. The first solvation layer contains twice as much physisorbed water molecules above the terraces, than chemisorbed ones located only at edges and corners. The solvent stabilizes the binding energy of chemisorbates.

Nanoparticles

Rodrigo Ferreira de Morais, Torsten Kerber, Federico Calle-Vallejo, Philippe Sautet, David Loffreda*

Capturing Solvation Effects at a Liquid/Nanoparticle Interface by Ab Initio Molecular Dynamics: Pt_{201} Immersed in Water